A DFT based equilibrium study on the hydrolysis and the dehydration reactions of MgCl2 hydrates

A DFT based equilibrium study on the hydrolysis and the dehydration reactions of MgCl2 hydrates

B. Smeets, E. Iype, S. V. Nedea, H. A. Zondag, and C. C. M. Rindt

Citation: J. Chem. Phys. **139**, 124312 (2013); doi: 10.1063/1.4822001
View online: http://dx.doi.org/10.1063/1.4822001
View Table of Contents: http://jcp.aip.org/resource/1/JCPSA6/v139/i12
Published by the AIP Publishing LLC.

A DFT based equilibrium study on the hydrolysis and the dehydration reactions of $MgCl_2$ hydrates

B. Smeets, E. Iype, S. V. Nedea,[a] H. A. Zondag, and C. C. M. Rindt
Energy Technology, Eindhoven University of Technology, The Netherlands

(Received 24 May 2013; accepted 9 September 2013; published online 30 September 2013)

Magnesium chloride hydrates are characterized as promising energy storage materials in the built-environment. During the dehydration of these materials, there are chances for the release of harmful HCl gas, which can potentially damage the material as well as the equipment. Hydrolysis reactions in magnesium chloride hydrates are subject of study for industrial applications. However, the information about the possibility of hydrolysis reaction, and its preference over dehydration in energy storage systems is still ambiguous at the operating conditions in a seasonal heat storage system. A density functional theory level study is performed to determine molecular structures, charges, and harmonic frequencies in order to identify the formation of HCl at the operating temperatures in an energy storage system. The preference of hydrolysis over dehydration is quantified by applying thermodynamic equilibrium principles by calculating Gibbs free energies of the hydrated magnesium chloride molecules. The molecular structures of the hydrates ($n = 0$, 1, 2, 4, and 6) of $MgCl_2$ are investigated to understand the stability and symmetry of these molecules. The structures are found to be noncomplex with almost no meta-stable isomers, which may be related to the faster kinetics observed in the hydration of chlorides compared to sulfates. Also, the frequency spectra of these molecules are calculated, which in turn are used to calculate the changes in Gibbs free energy of dehydration and hydrolysis reactions. From these calculations, it is found that the probability for hydrolysis to occur is larger for lower hydrates. Hydrolysis occurring from the hexa-, tetra-, and di-hydrate is only possible when the temperature is increased too fast to a very high value. In the case of the mono-hydrate, hydrolysis may become favorable at high water vapor pressure and at low HCl pressure. © *2013 AIP Publishing LLC*. [http://dx.doi.org/10.1063/1.4822001]

I. INTRODUCTION

Magnesium salt hydrates are potential candidate materials for seasonal energy storage systems in the built environment.[1] $MgCl_2 \cdot nH_2O$ and $MgSO_4 \cdot nH_2O$, where $n = \{1, 2, \ldots 6\}$, are particularly interesting due to their high energy storage densities (roughly 2–3 GJ/m^3)[2] and their wide availability. Solar energy collected in summer can be stored as the energy of dehydration, and in winter, the system is hydrated to retrieve the stored energy. However, the performance of such systems is dependent on the material properties and the kinetics of the hydration and dehydration reactions. The crystal structure, surface defects and dislocations present in these hydrates significantly influence the hydration/dehydration kinetics.[3] The $MgSO_4$ hydrates are known to exhibit slow kinetics, arguably due to the presence of meta-stable states,[4] whereas the hygroscopic magnesium chloride generally undergoes faster hydration and dehydration reactions, essentially increasing the power output in a seasonal energy storage system. However, the dehydration of $MgCl_2$ hydrates is usually accompanied by a hydrolysis[5] reaction with the release of HCl, which can potentially damage the material as well as the equipment.

Molecular structures of $MgSO_4$ hydrates have been subject of investigation in the literature,[6–13] especially the presence of strong hydrogen bond networks catalyzing the formation of meta-stable states.[6,7,14] However, fewer accounts exist on the molecular structure of $MgCl_2$ hydrates. Crystalline structures of the hygroscopic magnesium chloride hexa-hydrate (also known as Bischofite) are reported from Neutron Diffraction studies by Agron and Busing.[15] Sugimoto *et al.*[16] report X-ray diffraction studies for the crystalline refinement of three hydrates of magnesium chloride $MgCl_2 \cdot nH_2O$; ($n = 1$, 2, 4). In their experiments, they identified the presence of several phases of magnesium chloride hydrates during dehydration. However, most of these phases do not posses a distinguishable crystalline structure.[16] The most crystalline phase among these is the tetra-hydrate ($MgCl_2 \cdot 4H_2O$). A DFT (Density Functional Theory) study[17] reports the molecular structures of $MgCl_2 \cdot nH_2O$; ($n = 0$, 1, 2, 4, 6). Information about the crystalline structures of other hydrates ($n = 5$, 3) are not reported in the literature, suggesting that these hydrates are unstable.

Due to the industrial importance of the hydrates of $MgCl_2$,[18,19] a number of experimental studies have been performed on the dehydration reactions of $MgCl_2 \cdot 6H_2O$.[16,20] Magnesium chloride hexahydrate is the main raw material for the production of Mg metal by electrolysis of molten $MgCl_2$.[21] Often, the dehydration process for the production of anhydrous $MgCl_2$ from $MgCl_2 \cdot 6H_2O$ is challenging due to the release of HCl gas from the hydrolysis reaction.[20,22] Kelley[5] pointed out that hydrolysis is inevitable during the

[a]Electronic mail: s.v.nedea@tue.nl

dehydration of $MgCl_2 \cdot 6H_2O$. Many studies have been carried out to understand the process of hydrolysis during the dehydration step.[18,23–25] Hydrolysis in $MgCl_2$ hydrates is usually avoided by performing dehydration in the presence of HCl.[5,26] Alternative methods to the direct dehydration of $MgCl_2 \cdot 6H_2O$ are being proposed for the production of $MgCl_2$[27,28] in order to avoid hydrolysis. In energy storage systems, this hydrolysis reaction poses a challenge, due to the release of harmful HCl gas, to the salt hydrates as well as to the equipment. However, in most of the experiments mentioned above, the dehydration for industrial applications is performed at relatively high temperatures (above 600 K), whereas in seasonal energy storage systems, the dehydration is carried out at a maximum temperature of 450 K. Kirsh and Shoval,[25] in their experiment, did not see hydrolysis when dehydrating below 473 K, whereas Huang *et al.*[29] observed hydrolysis when calcining $MgCl_2 \cdot 6H_2O$ isothermally within the range from 440 K to 476 K. Partial hydrolysis was also observed at 473 K when dehydrating $MgCl_2 \cdot 4H_2O$ in the absence of HCl pressure. Thus, the information about the possibility of the hydrolysis reaction, and its preference over dehydration remains ambiguous. A study based on the thermodynamic equilibrium principles via the Gibbs free energy of the reactions is therefore necessary, to determine the preference of hydrolysis over dehydration, especially when the experimental observations remain inconclusive.

The objective of this study is to identify the formation of HCl at the operating temperatures in an energy storage system. The preference of hydrolysis over dehydration needs to be quantified by applying thermodynamic equilibrium principles. First, we study the molecular structures of the hydrates (n = 0, 1, 2, 4, and 6) of $MgCl_2$ to understand the stability and symmetry of each of the molecules. Subsequently, the frequency spectra of these molecules are used to study the equilibrium of the hydrolysis reactions. Changes in Gibbs free energy of various reactions are calculated and thereby equilibrium concentrations of the reactants and products are computed.

II. METHODOLOGY

DFT[30,31] using the generalized gradient approximation with the Perdew Wang 91 (PW91) functional[32] implemented in the Amsterdam Density Functional (ADF) program is used for computing the optimized structures and the energies of $MgCl_2 \cdot nH_2O$ (for n = 0, 1, 2, ... 6). This method is, successfully, applied for studying molecular systems involving magnesium,[7] chlorides,[33,34] and hydrogen bonds.[35] A spin-restricted Kohn-Sham method is used with a doubly polarized triple-ζ basis set, while keeping the integration accuracy to the maximum throughout the calculation. Molecular structures of the hydrates for n = 0, 1, 2, 4, 6 were optimized such that the final geometries resemble the atomic orientations in the crystalline structures reported in the literature[16] for the respective hydrates. In addition, the geometries of H_2O, HCl, and MgOHCl were also optimized using the same method. The harmonic frequencies were calculated for all the final geometries in order to find their vibrational contributions to the molecular energy and entropy. Bader charges[36] were also calculated for each atom in the final geometries to study the changes in the charge distribution around the atoms.

For the free energy calculation, the ideal poly-atomic gas assumption[37] is used for each molecule. In reality, the hydrated $MgCl_2$ reactants and products remain in the solid state except the water vapor and the HCl gas. The periodic unit cells of the hydrates include a large number of atoms (6, 24, 18, 30, and 42 for n = 0, 1, 2, 4, and 6, respectively), which makes it relatively expensive to calculate the energies of optimized geometries and, especially, the frequencies with a satisfactory accuracy. In addition, the crystal structure of MgOHCl is difficult to identify and therefore, little information is available about the structure of this product.[16] Nevertheless, in reality, the reactants and products may not be in pure crystalline states. It is regarded that hydrolysis is more likely to happen in the liquid phase compared to the solid phase,[20] and thus the equilibrium hydrolysis and dehydration curves obtained for molecular structures may be regarded as safety limits for the equilibrium temperatures in seasonal heat storage systems. These were the reasons for using gas phase molecular structures of the hydrates for this calculation instead of the crystalline structures. With this assumption, we try to extract as much information as possible about the behavior of the system during dehydration reactions.

The dehydration reactions considered for analysis are

$$MgCl_2 \cdot nH_2O \xrightarrow{heating} MgCl_2 \cdot (n-2)H_2O + 2H_2O \quad \{n = 6\,and\,4\},$$

$$MgCl_2 \cdot nH_2O \xrightarrow{heating} MgCl_2 \cdot (n-1)H_2O + H_2O \quad \{n = 2\,and\,1\}.$$

Hydrolysis reactions have been observed experimentally when the dehydration starts from $MgCl_2 \cdot 6H_2O$[29] as well as from $MgCl_2 \cdot 4H_2O$,[38] although, the most common observation is when dehydrating $MgCl_2 \cdot 2H_2O$.[5,20] Therefore, the hydrolysis steps considered in our study, assuming they are one-step reactions, include

$$MgCl_2 \cdot nH_2O \xrightarrow{heating} MgOHCl + (n-1)H_2O + HCl \quad \{n = 6, 4, 2, 1\}.$$

The change in Gibbs free energy is calculated as

$$\Delta G = \sum_p G_p - \sum_r G_r, \tag{1}$$

$$G(T, p) = U + pV - TS, \tag{2}$$

$$U(T) = U_{trans} + U_{rot} + U_{vib} + U_{ZPE} + U_{elec}, \tag{3}$$

$$S(T, p) = S_{trans} + S_{rot} + S_{vib}, \tag{4}$$

$$pV = nRT. \tag{5}$$

In these equations , T is the temperature, p is the absolute pressure, and V is the volume. The internal energy and the entropy are given by U and S, respectively, each consisting of a translational, rotational, and vibrational part. U_{elec} represents the ground state electronic energy of the molecules at 0 K and U_{ZPE} is the zero-point energy. The general expression for the

entropy and the internal energy can be written in terms of the canonical partition function, q, as shown in Eqs. (6) and (7), respectively,

$$S = R\ln q + RT\left(\frac{\partial \ln q}{\partial T}\right), \tag{6}$$

$$U = RT^2\left(\frac{\partial \ln q}{\partial T}\right). \tag{7}$$

The partition functions for the different contributions are given below[37]

$$q_{trans} = \frac{k_B T}{p}\left(\frac{2\pi M k_B T}{h^2}\right), \tag{8}$$

$$q_{rot}^{linear} = \frac{I}{\sigma}\frac{8\pi^2 k_B T}{h^2}, \tag{9}$$

$$q_{rot} = \frac{\sqrt{\pi I_a I_b I_c}}{\sigma}\left(\frac{8\pi^2 k_B T}{h^2}\right)^{\frac{3}{2}}, \tag{10}$$

$$q_{vib} = \prod_i \frac{1}{1-\exp\left(-h\nu_i/k_B T\right)}. \tag{11}$$

In the above equations, I_a, I_b, and I_c are the three principal moments of inertia of the molecules and ν_i represents the frequency for each vibrational mode i. M is the total mass of the molecule and σ is the symmetry number defined by the number of ways that the polyatomic molecule can be rotated into itself. The Boltzmann constant, Planck's constant, and the universal gas constant are, respectively, given by k_B, h, and R. Substituting Eqs. (8)–(11) into Eqs. (6) and (7) results in the expressions for the entropies and internal energies for the individual contributions, as shown below

$$S_{trans}(T,p) = R\left[\ln\left(\frac{k_B T}{p}\left(\frac{2\pi M k_B T}{h^2}\right)^{\frac{3}{2}}\right)+\frac{3}{2}\right], \tag{12}$$

$$S_{rot}(T) = R\left[\ln\left(\frac{\sqrt{\pi I_a I_b I_c}}{\sigma}\left(\frac{8\pi^2 k_B T}{h^2}\right)^{\frac{3}{2}}\right)+\frac{3}{2}\right], \tag{13}$$

$$S_{rot}^{linear}(T) = R\left[\ln\left(\frac{I}{\sigma}\frac{8\pi^2 k_B T}{h^2}\right)+1\right], \tag{14}$$

$$S_{vib}(T) = R\sum_{i=1}^{3N-6}\left[\frac{h\nu_i/k_B T}{\exp\left(h\nu_i/k_B T\right)-1}\right] - R\sum_{i=1}^{3N-6}\left[ln(1-\exp(-h\nu_i/k_B T))\right], \tag{15}$$

$$U_{trans}(T) = \frac{3}{2}RT, \tag{16}$$

$$U_{rot}(T) = \frac{3}{2}RT, \tag{17}$$

$$U_{rot}^{linear}(T) = RT, \tag{18}$$

$$U_{vib}(T) = R\sum_{i=1}^{3N-6}\left[\frac{h\nu_i/k_B}{\exp\left(h\nu_i/k_B T\right)-1}\right]. \tag{19}$$

The zero-point energy U_{ZPE} is calculated using Eq. (20)

$$U_{ZPE} = R\sum_{i=1}^{3N-6}\left[\frac{h\nu_i}{2k_B}\right]. \tag{20}$$

The principal moments of inertia and the vibrational frequencies are determined by DFT calculations and subsequently used to determine, respectively, the rotational and vibrational contributions to the internal energy and the entropy in addition to the zero-point energy.

III. RESULTS

A. Molecular structures of $MgCl_2 \cdot nH_2O$; ($n = 0, 1, 2, 4, 6$)

Figure 1 shows the optimized structure of the $MgCl_2$ molecule along with the bond lengths and the atomic charges. The structure is linear with the two Cl atoms separated by a Mg atom in the middle, which is similar to the crystalline structure of $MgCl_2$[16] as well as an *ab initio* study[39] reported in the literature. The Mg − Cl distance in the molecule is 2.18 Å after a geometry optimization which is also consistent with the literature.[39] The addition of a water molecule to the $MgCl_2$ molecule results in the structure of $MgCl_2 \cdot H_2O$, which is shown in Figure 2. This results in the bending of the Cl–Mg–Cl angle to 156.3° along with the stretching of the Mg − Cl bond to 2.21 Å. The coordination length between the Mg atom and the O atom in water is found to be 2.05 Å. The electronic energies, U_{elec}, of the structures are given in Figures 1–6.

For $MgCl_2 \cdot 2H_2O$, two structures were considered. The first structure is the lowest energy isomer as shown in Figure 3. This structure is slightly different from the known structure in the literature[16] of crystalline $MgCl_2 \cdot 2H_2O$. The structure in Figure 3 has a Cl − Mg–Cl angle of 146.1° along with an average Mg–Cl bond length of 2.265 Å. The structure involves two hydrogen bond interactions between both the water molecules and the two Cl atoms, and therefore the structure is not fully symmetric with respect to a plane passing through the Cl–Mg–Cl atoms. The other structure considered is a planar symmetric structure, as shown in Figure 4, which is consistent with the crystalline structure.[16] However,

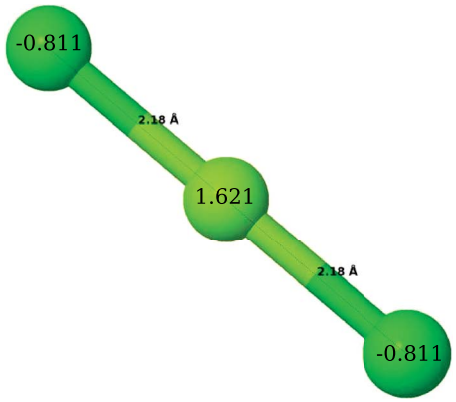

FIG. 1. Molecular structure of $MgCl_2$. $U_{elec} = -201.39$ kcal/mol. Atomic (Bader) charges and bond lengths are also given. Mg = *lime*, Cl = *green*.

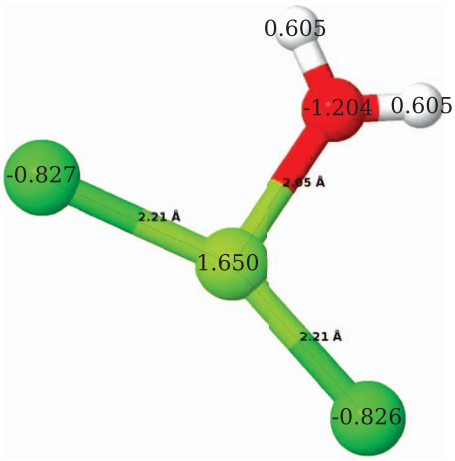

FIG. 2. Molecular structure of $MgCl_2 \cdot H_2O$. $U_{elec} = -553.73$ kcal/mol. Bond lengths and the atomic charges are given. Mg = *lime*, Cl = *green*, O = *red*, H = *white*.

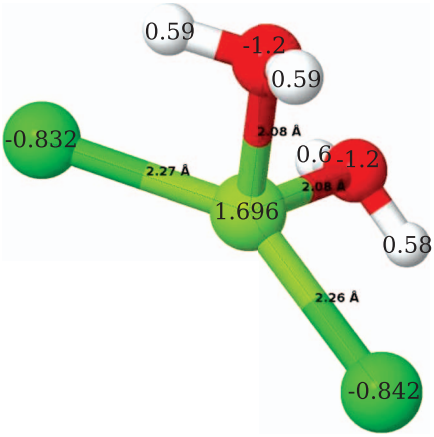

FIG. 3. Molecular structure of $MgCl_2 \cdot 2H_2O$. $U_{elec} = -903.94$ kcal/mol. Mg = *lime*, Cl = *green*, O = *red*, H = *white*.

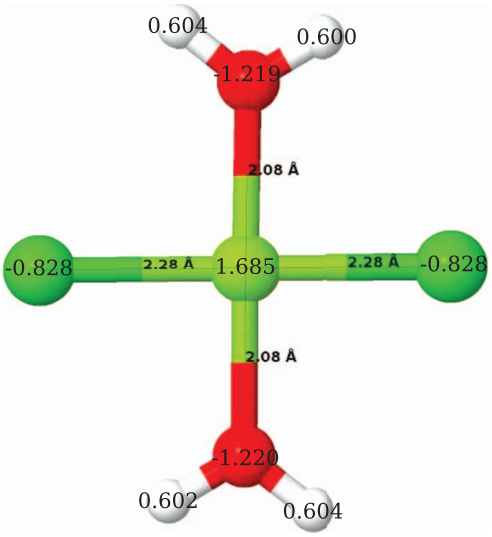

FIG. 4. Molecular structure of $MgCl_2 \cdot 2H_2O$ with planar symmetry. $U_{elec} = -899.38$ kcal/mol. Atomic charges and bond lengths are also given. Mg = *lime*, Cl = *green*, O = *red*, H = *white*.

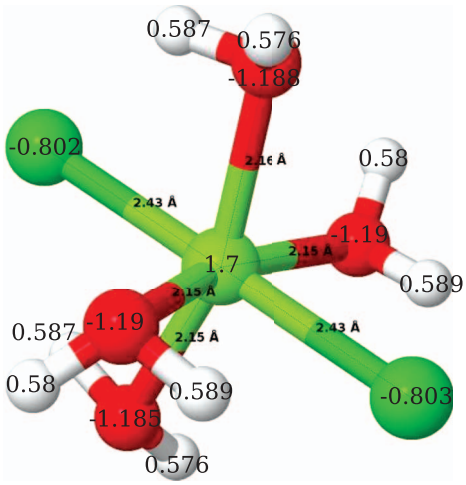

FIG. 5. Molecular structure of $MgCl_2 \cdot 4H_2O$. $U_{elec} = -1592.53$ kcal/mol. Atomic charges and bond lengths are also given. Mg = *lime*, Cl = *green*, O = *red*, H = *white*.

this planar symmetric structure possesses an imaginary frequency corresponding to the rotation of the H_2O molecules with respect to the axis passing through the O atoms, parallel to the Cl–Mg–Cl atoms. The bond lengths in the two structures of $MgCl_2 \cdot 2H_2O$ are not significantly different. We will use the planar symmetric geometry of Figure 4 (discarding the imaginary frequency) for the Gibbs free energy calculation in order to make sure that our calculation is consistent with crystalline structures. Bader charges for Mg in these structures seem to have slightly increased from 1.62 (Figure 1) to 1.68 (Figure 4), while the charges for Cl atoms increased only 0.02. Overall charge transfer appears to be negligibly small and therefore, the coordination between water molecules and the Mg atoms may be considered as more of a Coulombic interaction.

For the structure with four water molecules, Figure 5, an octahedral geometry is obtained after optimization with four water molecules on the plane and both the Cl atoms at the axial positions. The shape of this structure is in accordance with experimental observations.[16] The Mg–Cl bond length is

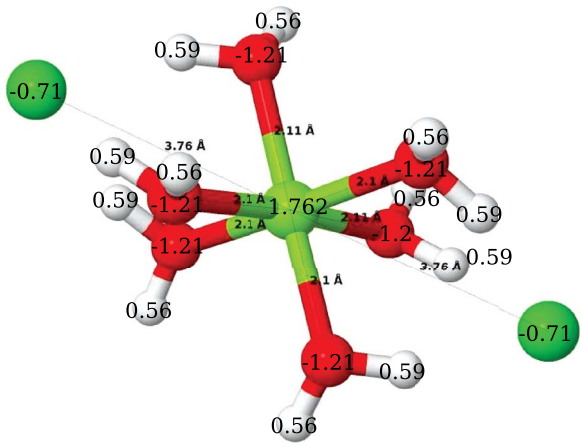

FIG. 6. Molecular structure of $MgCl_2 \cdot 6H_2O$. $U_{elec} = -2281.90$ kcal/mol. Atomic charges and bond lengths are also given. Mg = *lime*, Cl = *green*, O = *red*, H = *white*.

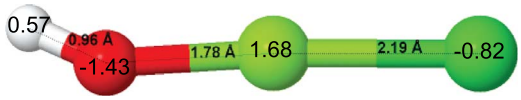

FIG. 7. Molecular structure of MgOHCl. $U_{elec} = -373.61$ kcal/mol. Atomic charges and bond lengths are also given. Mg = *lime*, Cl = *green*, O = *red*, H = *white*.

increased to 2.43 Å. The four water molecules have an average coordination length of 2.15 Å. This octahedral distortion is due to the larger size of the Cl atom compared to the O atom in water and not due to the Jahn-Teller distortion.[40] The structure in Figure 5 is not symmetric, but the octahedron is distorted by the influence of hydrogen bonds between water and Cl atoms. Thus, hydrogen bonds appear to have a small influence on the structures of $MgCl_2$ hydrates, but not as much as compared to $MgSO_4$ hydrates.[7] Also, the hydrates of $MgCl_2$ appear to be noncomplex without the presence of any unusual low energy isomers. This difference in the influence of hydrogen bonds to form meta-stable states may possibly be regarded as the reason for the faster hydration kinetics in $MgCl_2$ as observed by Ferchaud *et al.*[41] in comparison with $MgSO_4$.

For the optimized hexahydrate molecule of $MgCl_2$, Figure 6, the water molecules seem to be at the corners of a regular octahedron and the two chlorine atoms are placed along the axial direction, although the Cl atoms are not bonded to the Mg atom. The two chlorine atoms are, clearly, stabilized by the hydrogen bonds formed with the coordinated water molecules. Along with the significant change in the interaction length between Mg and Cl, the charge around the Cl atom is also decreased to −0.71. Song *et al.*[42] reports another isomer of $MgCl_2 \cdot 6H_2O$, where the water molecules are stabilized at three different levels with three different coordination lengths. In their study, at least two water molecules were not coordinated directly with the Mg atom. Formation of such isomers may be caused by the presence of hydrogen bonds. Nevertheless, the $MgCl_2 \cdot 6H_2O$ structure obtained in this study appears to be closer to the experimentally predicted octahedral structure of $MgCl_2 \cdot 6H_2O$.[16]

Figure 7 shows the optimized structure of the MgOHCl molecule along with its bond lengths and atomic charges. The Mg–Cl bond length and the atomic charge of the Cl atom are close to those in the structure of $MgCl_2$. On the other side of the Mg atom, the OH fragment is bonded with an Mg–O bond length of 1.78 Å. The magnitude of atomic charges of the Mg atom and the O atom are larger than is seen for the $MgCl_2$ hydrates, resulting in a smaller Mg–O bond length. Due to the low crystallinity of this material, the crystal structure of MgOHC*l* could not be determined experimentally.[16] Therefore, various initial geometries are considered in order to find the lowest energy isomer, all resulting in the same structure as given in Figure 7. The Cl–Mg–O bond angle is nonlinear with an angle of 176.1°, and the H–O–Mg bond angle is 148.2°.

The energies of the chemical reactions for dehydration and hydrolysis are shown in Table I. The dehydration energies, $\Delta E_{dehydration}$, per release of water molecule are calculated using the equations below:

TABLE I. Energies of the molecules and the dehydration (per release of water molecule) and hydrolysis reactions.

Molecule	Energy (kcal/mol)	$\Delta E_{dehydration}$ (kcal/mol)	$\Delta E_{hydrolysis}$ (kcal/mol)
$MgCl_2 \cdot 6H_2O$	− 2281.9	14.8	119.3
$MgCl_2 \cdot 4H_2O$	− 1592.5	16.7	89.7
$MgCl_2 \cdot 2H_2O$	− 899.4	15.7	46.3
$MgCl_2 \cdot H_2O$	− 553.7	22.4	40.5

$$\Delta E_{dehydration} = \begin{cases} 0.5 \times E_{MgCl_2.(n-2)H_2O} + \\ E_{H_2O} - 0.5 \times E_{MgCl_2.nH_2O}, & \text{if } n = 6, 4 \\ E_{MgCl_2.(n-1)H_2O} + \\ E_{H_2O} - E_{MgCl_2.nH_2O}, & \text{if } n = 2, 1 \end{cases}$$

Similarly, the hydrolysis energies, $\Delta E_{hydrolysis}$, are given by

$$\Delta E_{hydrolysis} = E_{MgOHCl} + (n-1) \times E_{H_2O} + E_{HCl} - E_{MgCl_2.nH_2O.} \quad (21)$$

In the above equations, the energies of stand alone H_2O and HCl molecules (i.e., $E_{H_2O} = -329.8$ kcal/mol and $E_{HCl} = -139.6$ kcal/mol) are used. It can be seen that, during the dehydration process, the first two water molecules are the easiest to be removed because the energy of dehydration of the first step is the lowest. The third, fourth, and fifth also have similar dehydration energies. The last water molecule is the most difficult to be removed. Looking at the fourth column in Table I, the energies of hydrolysis reactions are lower for lower hydrates. This is consistent with experimental evidences, which shows that the chances of hydrolysis is more for lower hydrates.

B. Vibrational frequency spectra

The O–H and Mg–Cl vibrational frequencies are plotted in Figures 8 and 9. The calculated peak positions for the H_2O molecule correspond well with the results found in the literature.[43] The eigen modes corresponding to the Mg–Cl, Mg–O, and O–H vibrations are indicated specifically in the figures for clarity. From Figure 8, it follows that the O–H vibrational frequencies in the molecules did not change when n (the hydration number) is increased from 1 to 2. However, the peak corresponding to symmetric stretch has been shifted to the left for $n = 4$ and still further for $n = 6$, presumably due to the influence of hydrogen bonds in the molecule.[44] In Figure 9, the asymmetric stretch of the Mg–Cl vibrations was shifted to the left from $n = 0$ to $n = 2$. In the case of $MgCl_2 \cdot 6H_2O$, the intensity of the Mg–Cl vibration, denoted with the ○ marker, is almost zero. The Cl atoms are stabilized by the H atoms by hydrogen bonds. Therefore, this vibration may be interpreted as the hydrogen bond vibrations between $[Mg(H_2O)_6]^{2+}$ and Cl^{2-} instead of Mg–Cl vibration, thus resulting in an increased frequency compared to the Mg–Cl stretch in the case of $MgCl_2 \cdot 4H_2O$. The peak

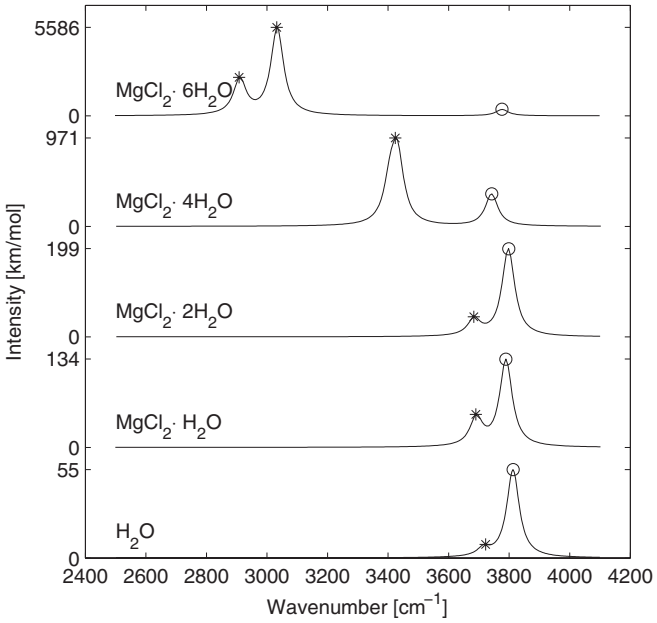

FIG. 8. IR spectra of the hydrates in the O–H frequency range. The signs indicate symmetric O–H stretch (∗) and asymmetric O–H stretch (○).

corresponding to Cl–Mg–Cl bend, marked with ×, disappears in Figure 9.

C. Equilibrium curves for dehydration reactions

From Eq. (1), it is understood that the change in Gibbs free energy ΔG for a reaction is a function of temperature T and pressure p, i.e., $\Delta G = \Delta G(T, p)$. At equilibrium, $\Delta G = 0$, which implies that we can calculate the equilibrium pressure of the reactants and products as a function of temperature, i.e., $p = p(T)$. Such equilibrium curves for the

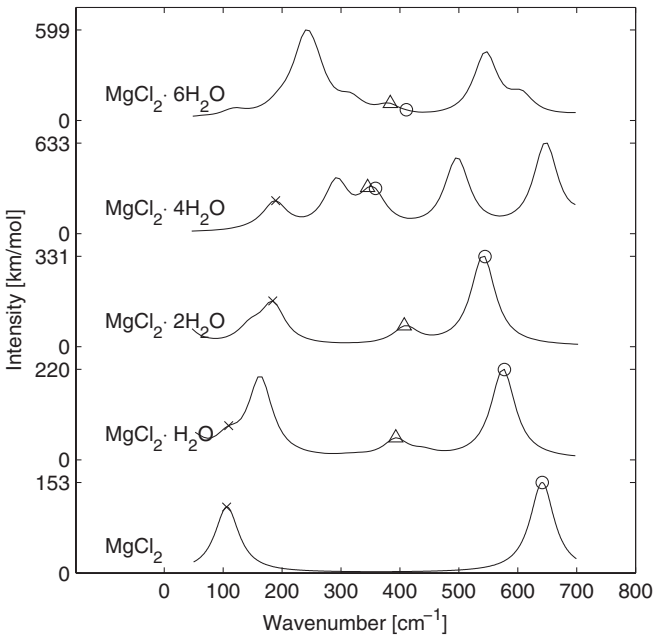

FIG. 9. IR spectra of the hydrates in the Mg–Cl vibrations range. The signs indicate Cl–Mg–Cl bend (×), Mg–Cl stretch (○), and Mg–O stretch (△).

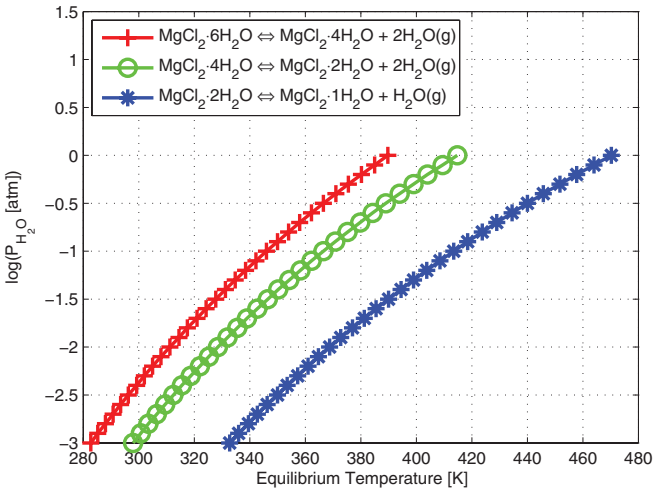

FIG. 10. Equilibrium water vapor pressures for the dehydration reactions of the $MgCl_2$ hydrates.

dehydration reactions, mentioned in the introduction, are calculated to show the effect of temperature and pressure on the reaction equilibrium. Figure 10 shows the equilibrium water vapor pressure vs temperature for the three dehydration reactions: (from hexa-hydrate to tetra-hydrate, from tetra-hydrate to di-hydrate and from di-hydrate to mono-hydrate). In this calculation, only the partial pressure of H_2O is changed and the partial pressures of the hydrates are kept constant at 1 atm. In real experiments, only the partial pressures of H_2O and sometimes HCl are the controlled variables and the changes in concentrations of the hydrates are not important. This is the reason for using constant hydrates pressure.

The equilibrium curves in Figure 10 match approximately with the results found in the literature.[5,20] According to Figure 10, the dehydration of higher hydrates occurs at lower temperatures and vice versa for lower hydrates, which is consistent with experiments.[5,20] In addition, the slopes of the equilibrium lines are equal to those found in the literature. However, an offset of 25 K is observed in the temperature axis in Figure 10 compared to values found in the literature. This difference may be the consequence of the ideal poly-atomic gas assumption involved in the calculation. From the curves, it may be understood that the first two reaction steps in the dehydration mechanism proceed relatively at ease (lower temperatures) within the temperature range of interest. The figure shows that the dehydration becomes increasingly difficult as the water vapor pressure increases.

D. Equilibrium curves for hydrolysis reactions

A similar analysis is performed to obtain the equilibrium curves for the hydrolysis reactions starting from hexa-hydrate, tetra-hydrate, di-hydrate, and the mono-hydrate. Figure 11 shows the equilibrium water vapor pressure as a function of temperature for the four hydrolysis reactions, in which the HCl pressure is kept constant at 0.001 atm for this calculation. The concave curves show that the hydrolysis reaction is increasingly difficult as the water vapor pressure increases. The hydrolysis reaction for the mono-hydrate does

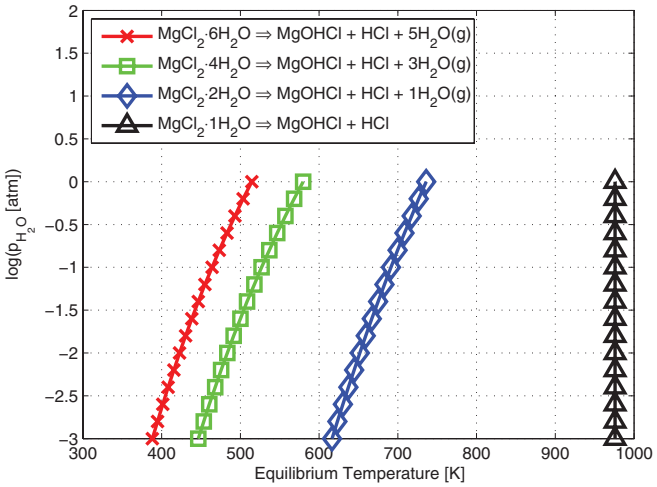

FIG. 11. Equilibrium H_2O pressures for the hydrolysis reactions of the $MgCl_2$ hydrates. $p_{HCl} = 0.001$ atm.

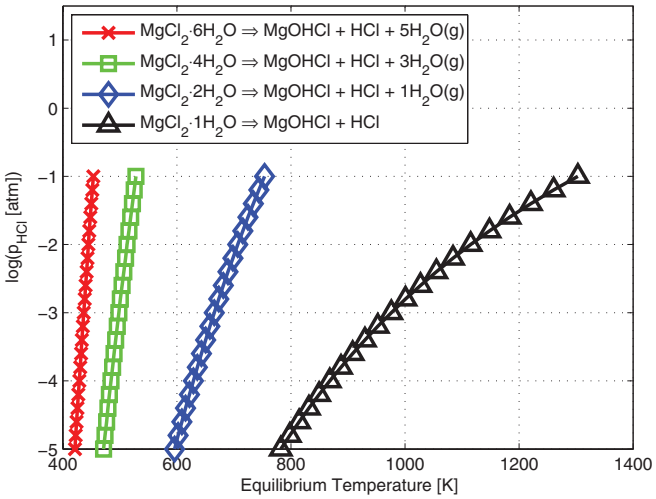

FIG. 12. Equilibrium HCl pressures for the hydrolysis reactions of the $MgCl_2$ hydrates. $p_{H_2O} = 0.023$ atm.

not depend on the water vapor pressure as water vapor is not a product of the reaction. Therefore, the corresponding equilibrium curve is a vertical line in Figure 11.

Comparing Figures 10 and 11, it can be seen that at a given water vapor pressure and HCl pressure, the equilibrium temperatures for the hydrolysis reactions are higher than those for the dehydration reactions. This implies that the dehydration reaction is always favorable compared to the hydrolysis reaction for this HCl pressure of 0.001 atm. Another observation is that the equilibrium temperature difference between the hydrolysis reaction and the dehydration reaction for a given water vapor pressure, or in other words, the offset of the hydrolysis line in Figure 11 with respect to the dehydration line in Figure 10 for each hydrate, decreases with the hydration number. From this, one should expect that hydrolysis becomes less favorable for lower hydrates. However, experiments do show that hydrolysis happens mostly for the lower hydrates. Now, Figure 12 shows the changes in the equilibrium HCl pressure as a function of temperature for the hydrolysis reactions with the H_2O pressure kept constant at $p_{H_2O} = 0.023$ atm. From Figure 12, it can be seen that the changes in the equilibrium temperature is more for lower hydrates for a given change in the HCl pressure. This is because the molar ratio between HCl and H_2O in the hydrolysis products increases with a decrease in hydration number. This implies that lowering the HCl pressure indeed favors the hydrolysis reaction for lower hydrates and thus decreases the temperature offset between the hydrolysis and the dehydration reaction, so that it eventually becomes smaller for the lower hydrates. This is the reason why we observe more hydrolysis for lower hydrates, which is consistent with experiments.[5,20,24,38]

E. Preference of hydrolysis over dehydration

A comparison between the hydrolysis reaction and the dehydration reaction, to understand the preference of one over the other for different combinations of HCl and H_2O pressures, is shown here. Figure 13 shows the equilibrium lines for the dehydration reaction as well as the hydrolysis reaction of the magnesium chloride mono-hydrate. It shows the equilibrium water vapor pressure as function of the temperature for different HCl pressures. It can be seen that the equilibrium temperature decreases as the HCl pressure is decreased. In principle, hydrolysis becomes favorable when the HCl pressure becomes low, such that the hydrolysis curve crosses over to the left of the dehydration curve. For instance, the maximum HCl pressure required for the hydrolysis curve to cross the dehydration curve, at $p_{H_2O} = 0.023$ atm, is about $p_{HCl} = 10^{-7}$ atm. Similarly, the maximum HCl pressures below which the hydrolysis becomes favorable for the di-, tetra-, and hexa-hydrate, at $p_{H_2O} = 0.023$ atm, are 10^{-17}, 10^{-21}, and 10^{-25} atm, respectively. Thus the equilibrium curve analysis shows here that the hydrolysis reactions are, usually, thermodynamically less favorable compared to dehydration reactions especially in the operating conditions of a seasonal energy storage system.

Figure 14 shows the equilibrium H_2O and HCl pressures for the dehydration and hydrolysis reaction for $MgCl_2 \cdot H_2O$

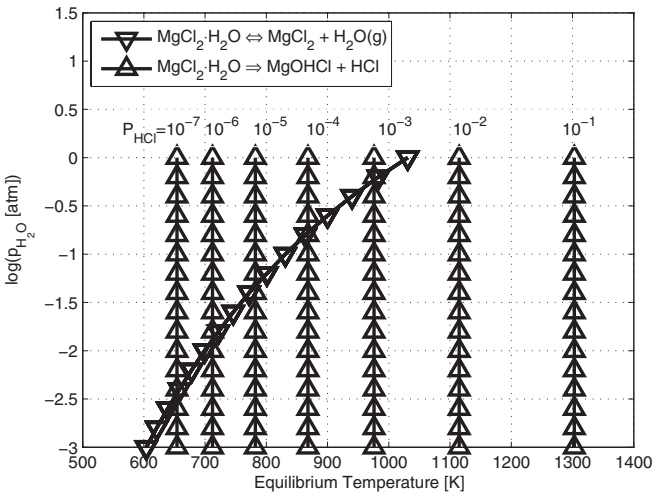

FIG. 13. Equilibrium H_2O pressures for both reactions for $MgCl_2 \cdot H_2O$. The HCl pressure is varied from 10^{-7} to 10^{-1} atm.

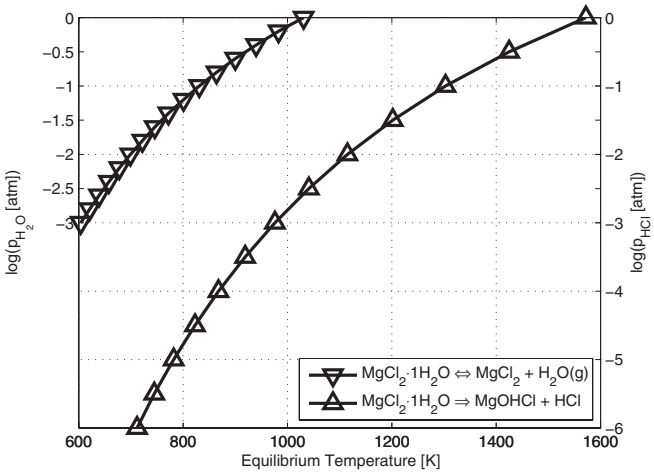

FIG. 14. Equilibrium H_2O and HCl pressures for the dehydration and hydrolysis reaction for $MgCl_2 \cdot 1H_2O$ as a function of temperature.

as a function of temperature. Since only either one of the products between H_2O and HCl will be formed for these reactions, the curves should be viewed with the correct pressure axis. The equilibrium HCl pressure for the hydrolysis reaction is given on the right axis in Figure 14, while the equilibrium H_2O pressure for the dehydration reaction is given on the left axis. From this figure, it can be seen that hydrolysis is favorable if the equilibrium temperature of the hydrolysis reaction is lower than the equilibrium temperature of the dehydration reaction. Each equilibrium temperature is related to particular values of HCl and H_2O pressures. The line in Figure 15 corresponds to the combinations of HCl and H_2O pressures with equal equilibrium temperatures. Therefore, any combination of pressures on the left side of the line will result in a condition favoring dehydration reaction, and any combination on the right side of the line will result in a condition favoring the hydrolysis reaction.

Overall one can say that hydrolysis occurring from the hexa-, tetra-, and di-hydrate is only possible when the temperature is increased too fast to a high value. For instance, if the temperature is increased in order to dehydrate the lower hydrates when at the same time, the higher hydrates are also present, the temperature might reach towards the maximum value for hydrolysis to occur from the higher hydrates. Even then, the dehydration reaction remains favorable at every temperature and pressure. However, in the case of the mono-hydrate, hydrolysis may become favorable at high water vapor pressure, which will counteract the dehydration reaction, and at very low HCl pressure, which will favor the hydrolysis reaction. Despite this, if a little HCl is formed and the HCl pressure rises, it thwarts the formation of more HCl.

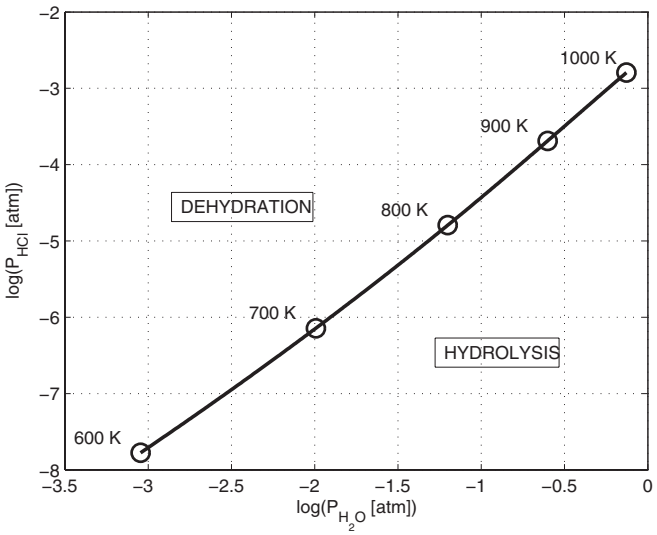

FIG. 15. preference of reaction for $MgCl_2 \cdot H_2O$ for different combinations of HCl pressures and H_2O pressures with equal equilibrium temperatures.

IV. CONCLUSION

Molecular structures of $MgCl_2 \cdot nH_2O$, where $n = \{0, 1, 2, 4, \text{and } 6\}$, were analyzed along with the atomic charges in order to understand the equilibrium curves for dehydration and hydrolysis reactions observed in these salt hydrates. Harmonic frequencies were calculated for the geometries, and thereby the Gibbs free energies of the dehydration and the hydrolysis reaction are used to generate the equilibrium curves. From the molecular structures of the hydrates, it can be seen that the hydrogen bonds existing in the geometries are relatively weak with almost no meta-stable isomers. This probably may be related to the faster kinetics observed in the hydration of chlorides compared to sulfates. Gibbs free energy calculations are performed to study the preference of hydrolysis over dehydration reactions. It is found that the probability for hydrolysis to occur is larger for lower hydrates. Hydrolysis occurring from the hexa-, tetra-, and di-hydrate is only possible when the temperature is increased too fast to a very high value. In the case of the mono-hydrate, hydrolysis may become favorable at high water vapor pressure and at low HCl pressure.

ACKNOWLEDGMENTS

The authors are grateful to National Computing Facility-SARA for proving the necessary computational resources.

[1] V. van Essen, H. Zondag, J. C. Gores, L. Bleijendaal, M. Bakker, R. Schuitema, W. van Helden, Z. He, and C. C. M. Rindt, J. Sol. Energy Eng. **131**, 041014 (2009).
[2] K. E. N'Tsoukpoe, H. Liu, N. L. Pierrés, and L. Luo, Renewable Sustainable Energy Rev. **13**, 2385 (2009).
[3] M. A. Stanish and D. D. Perlmutter, AIChE J. **30**, 557 (1984).
[4] S. J. Chipera and D. T. Vaniman, Geochim. Cosmochim. Acta **71**, 241 (2007).
[5] K. K. Kelley, *Energy Measurements and Equilibria in the Dehydration, Hydrolysis, and Decomposition of Magnesium Chloride* (U. S. Government Printing Office, 1945).
[6] G. M. Chaban, W. M. Huo, and T. J. Lee, J. Chem. Phys. **117**, 2532 (2002).
[7] E. Iype, S. V. Nedea, C. C. M. Rindt, A. A. van Steenhoven, H. A. Zondag, and A. P. J. Jansen, J. Phys. Chem. C **116**, 18584 (2012).
[8] G. Ferraris, D. W. Jones, and J. Yerkess, J. Chem. Soc., Dalton Trans. **1973**, 816.
[9] S. Aleksovska, V. M. Petrusevski, and B. Soptrajanov, Acta Crystallogr., Sect. B: Struct. Sci. **54**, 564 (1998).
[10] A. D. Fortes, I. G. Wood, L. V. Vočadlo, H. E. A. Brand, and K. S. Knight, J. Appl. Crystallogr. **40**, 761 (2007).
[11] P. J. Rentzeperis and C. T. Soldatos, Acta Crystallogr. **11**, 686 (1958).
[12] W. H. Baur, Acta Crystallogr. **17**, 863 (1964).

[13]A. S. Batsanov, Acta Crystallogr., Sect. C: Cryst. Struct. Commun. **56**, e230 (2000).
[14]A. Zalkin, H. Ruben, and D. H. Templeton, Acta Crystallogr. **17**, 235 (1964).
[15]P. A. Agron and W. R. Busing, Acta Crystallogr., Sect. C: Cryst. Struct. Commun. **41**, 8 (1985).
[16]K. Sugimoto, R. E. Dinnebier, and J. C. Hanson, Acta Crystallogr., Sect. B: Struct. Sci. **63**, 235 (2007).
[17]G. Liu, X. Song, and J. Yu, Mater. Sci. Forum **488**, 53 (2005).
[18]S. Kashani-Nejad, K.-W. Ng, and R. Harris, Metall. Mater. Trans. B **36**, 153 (2005).
[19]D. Eliezer, E. Aghion, and F. Froes, Adv. Perform. Mater **5**, 201 (1998).
[20]G. J. Kipouros and D. R. Sadoway, J. Light. Met. **1**, 111 (2001).
[21]R. Lastra, Trans. Inst. Min. Metall., Sect. C **100**, 110 (1991).
[22]W. Yu-Long, H. Xiao-Fang, Y. Ming-De, Z. Shu-Ping, D. Jie, and H. Hu-Sheng, J. Anal. Appl. Pyrolysis **81**, 133 (2008).
[23]T. J. Gardner and G. L. Messing, Thermochim. Acta **78**, 17 (1984).
[24]A. K. Galwey and G. M. Laverty, Thermochim. Acta **138**, 115 (1989).
[25]Y. Kirsh, S. Yariv, and S. Shoval, J. Therm. Anal. **32**, 393 (1987).
[26]H. Moscowitz, D. Lando, and D. Wolf, Ind. Eng. Chem. Prod. Res. Dev. **17**, 156 (1978).
[27]M. I. Pownceby, D. H. Jenkins, R. Ruzbacky, and S. Saunders, J. Chem. Eng. Data **57**, 2855 (2012).
[28]Z. Zhang, X. Lu, S. Yang, and F. Pan, Ind. Eng. Chem. Res. **51**, 9713 (2012).
[29]Q. Huang, G. Lu, J. Wang, and J. Yu, J. Anal. Appl. Pyrolysis **91**, 159 (2011).
[30]P. Hohenberg and W. Kohn, Phys. Rev. **136**, B864 (1964).
[31]W. Kohn and J. L. Sham, Phys. Rev. **140**, A1133 (1965).
[32]J. P. Perdew, Physica B **172**, 1 (1991).
[33]S. G. Podkolzin, E. E. Stangland, M. E. Jones, E. Peringer, and J. A. Lercher, J. Am. Chem. Soc. **129**, 2569 (2007).
[34]T. A. Baker, C. M. Friend, and E. Kaxiras, J. Chem. Phys. **130**, 084701 (2009).
[35]J. Ireta, J. Neugebauer, and M. Scheffler, J. Phys. Chem. A **108**, 5692 (2004).
[36]R. Bader, *Atoms in Molecules: A Quantum Theory* (Oxford university Press, New York, 1990).
[37]D. A. McQuarrie, *Statistical Mechanics* (University Science Books, Sausalito, CA, USA, 2003).
[38]H.-C. Eom, H. Park, and H.-S. Yoon, Adv. Powder Technol. **21**, 125 (2010).
[39]K. Eichkorn, U. Schneider, and R. Ahlrichs, J. Chem. Phys. **102**, 7557 (1995).
[40]H. A. Jahn and E. Teller, Proc. R. Soc. London, Ser. A **161**, 220 (1937).
[41]C. J. Ferchaud, H. A. Zondag, J. B. J. Veldhuis, and R. de Boer, J. Phys: Conf. Ser. **395**, 012069 (2012).
[42]X. Song, G. Liu, Z. Sun, and J. Yu, Asia-Pac. J. Chem. Eng. **7**, 221 (2012).
[43]"See http://www.ansyco.de/ for information about the IR spectra of H_2O.
[44]K. Nakamoto, M. Margoshes, and R. E. Rundle, J. Am. Chem. Soc. **77**, 6480 (1955).